Surface Granular flows: Two Related Examples

D. V. Khakhar† and Ashish V. Orpe

Department of Chemical Engineering, Indian Institute of Technology - Bombay, Powai, Mumbai 400076, India

J. M. Ottino

Department of Chemical and Mechanical Engineering, Northwestern University, Evanston, IL 60208, USA

(Dated: July 26, 2001)

Granular surface flows are common in industrial practice and natural systems, however, theoretical description of such flows is at present incomplete. Two prototype systems involving surface flow are compared: heap formation by pouring at a point and rotating cylinders. Continuum models for analysis of these flows are reviewed, and experimental results for quasi-2d systems are presented. Experimental results in both systems are well described by continuum models.

I. INTRODUCTION

Granular flows have been the subject of considerable recent work [1–5] driven by both technological needs [6, 7] and the recognition that many aspects of the basic physics are poorly understood [8]. Surface flows of granular materials, that is flows confined to a surface layer on a static granular bed, are important in industrial practice and nature. Industrial examples appear in the transportation, processing and storage of materials in systems such as rotary kilns, tumbling mixers, and feeding and discharge of silos. Examples in nature include the formation of sand dunes, lava flow, avalanches, and transport of sediments in rivers. Although considerable progess has been made, theoretical description of surface flows is incomplete at present. Several approaches, based on different assumptions about the physics of the flows, have been proposed [9–19]. A few experimental studies are also available [9, 13, 19–30]. Most work is focussed on two systems: heap formation and rotating cylinders shown schematically in Fig. 1. In the case of a heap, the surface flow is generated by pouring at a point.

An important feature of surface granular flows is the interchange of particles between the flowing layer and the fixed bed. In the case of a rotating cylinder the interchange rate is determined by kinematics since the velocity of the fixed bed at the bed-layer interface is known. The situation in the case of heap flow is more complicated. Bouchaud *et al.* [12] proposed a phenomenological model (BCRE model) in which the interchange rate is determined by the local surface angle. A variation of this model proposed by Boutreux *et al.* [16] (BRdG model)

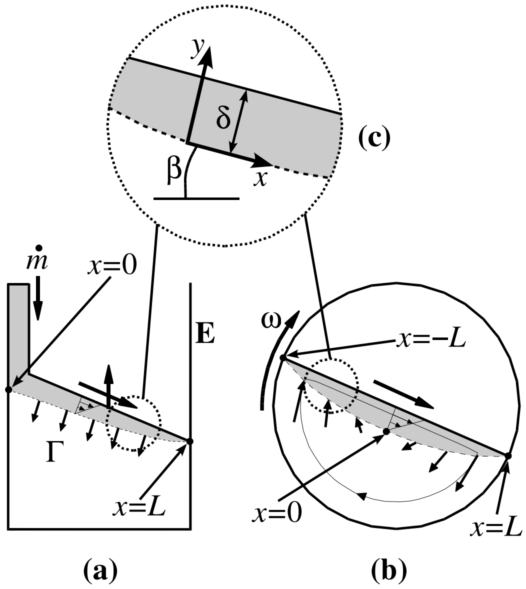

FIG. 1: Schematic view of surface flow systems: (a) Heap flow (b) Rotating cylinder flow. (c) Coordinate system used in the analysis.

has been broadly validated by continuum models [18, 19] and experiments [19], as we show below. Continuum models developed previously, for both heaps and rotating cylinders, are all based on depth-averaged hydrodynamic equations and differ primarily in the constitutive equations used. All the models contain parameters which must be evaluated from experiments. However, in most cases, these parameters have not been determined and comparisons of model predictions to experiments have not been reported. Hence the validity of the models is not known.

Here we present here a common continuum based

†`khakhar@iitb.ac.in`

framework for the analysis of both heap flow and rotating cylinder flow. The treatment closely follows that given in refs. [19] and [30]. Model predictions are compared to experimental results and to predictions of previous models. The general continuum model is presented first. Results for the heap formation and rotating cylinder flow are given next followed by conclusions.

II. GENERAL ONTINUUM MODEL

Consider a flowing layer on the surface of a granular bed assuming the flow is nearly uni-directional in the layer and curvature effects are small. The depth averaged equations for flow in the layer are then, the continuity equation

$$\frac{\partial}{\partial t}\left(\delta\langle\rho\rangle\right)+\frac{\partial}{\partial x}\left(\delta\langle\rho v_x\rangle\right)=\left(\rho v_y\right)|_{y=0}, \qquad (1)$$

and the x-momentum balance equation

$$\frac{\partial}{\partial t}\left(\delta\langle\rho v_x\rangle\right)+\frac{\partial}{\partial x}\left(\delta\langle\rho v_x^2\rangle\right)=-\frac{\partial}{\partial x}\left(\delta\langle\tau_{xx}\rangle\right)+\tau_{xy}|_{y=0}+\left(\rho v_x v_y\right)|_{y=0}+\langle\rho\rangle g\delta\sin\beta. \qquad (2)$$

In the above equations, v_x and v_y are the velocity components, τ_{xy} and τ_{xx} the shear stress and normal stress, ρ the bulk density of solids, $\beta(x,t)$ is the angle made by the interface with the horizontal, and $\langle\cdot\rangle=(1/\delta)\int_0^\delta \cdot dy$ denotes an average across the layer.

A number of assumptions are required to simplify eqs. (1) and (2). Here we take the bulk density in the layer (ρ) to be nearly constant (since the dilation of the flowing particles is not too large in the relatively slow flows being considered), and the velocity profile in the layer to be linear and of the form

$$v_x=2u(x,t)\frac{y}{\delta}, \qquad (3)$$

where $u=\langle v_x\rangle$ is the depth averaged velocity in the layer. The variation of the normal stress (τ_{xx}) in the flow direction (x) is neglected considering that changes in the layer thickness are small. Based on recent empirical evidence [30], the shear stress is taken to be

$$\tau_{xy}|_{y=0}=-c\rho d\delta\left(\frac{\partial v_x}{\partial y}\right)^2-\rho g\delta\cos\beta\tan\beta_s \qquad (4)$$

where $c\approx 1.5$ is a parameter of the model, d is the particle diameter and $\tan\beta_s$ is the effective coefficient of *dynamic* friction, with β_s taken to be the static angle of repose. Using the above assumptions, the governing equations reduce to

$$\frac{\partial\delta}{\partial t}+\frac{\partial}{\partial x}\left(\delta u\right)=-\Gamma, \qquad (5)$$

$$\frac{\partial}{\partial t}\left(\delta u\right)+\frac{4}{3}\frac{\partial}{\partial x}\left(\delta u^2\right)=-cd\frac{u^2}{\delta}+g\delta\frac{\sin(\beta-\beta_s)}{\cos\beta_s}, \qquad (6)$$

where $\Gamma=-v_y|_{y=0}$. Further, assuming the static friction forces at the heap-layer interface to be fully mobilized, the Mohr-Coulomb criterion yields

$$\tau_{xy}|_{y=0}=-\rho g\delta\cos\beta\tan\beta_m, \qquad (7)$$

where $\tan\beta_m$ is the effective coefficient of *static* friction. The experimental technique for measurement of β_m is discussed below.

Using eq. (4) and the assumptions given above, eq. (7) yields

$$u=\dot\gamma\delta/2, \qquad (8)$$

with the shear rate ($\dot\gamma=\partial v_x/\partial y$) given by

$$\dot\gamma=\left[\frac{g\cos\beta\sin(\beta_m-\beta_s)}{cd\cos\beta_m\cos\beta_s}\right]^{1/2}. \qquad (9)$$

Finally, the dynamics of the interface motion is given by

$$\frac{\partial h}{\partial t}=\Gamma\cos\beta,\qquad \frac{\partial h}{\partial x}=-\sin\beta,\qquad \frac{\partial w}{\partial x}=\cos\beta, \qquad (10)$$

where $(h(x,t),w(x,t))$ gives the parametric equation for the interface (Fig. 1). This completes the formulation of the model and all variables (u, δ, β, Γ, h, w) can be calculated using (eqs. 5,6,8-10) and appropriate initial and boundary conditions.

A similar analysis is given by Douady *et al.* [18]. An important difference is that Douady *et al.* [18] do not include a constitutive equation for stress in the flowing layer (equivalent to eq. 4). Instead, the shear rate in the flowing layer is assumed to be constant as opposed to (eq. 9). The application of these results to the case of heap flow and rotating cylinder flow is considered in the following sections.

III. HEAP FORMATION

Consider a quasi-steady flow ($\partial\delta/\partial t,\partial u/\partial t\approx 0$) and a slowly varying interface angle ($\partial\beta/\partial x\approx 0$) during heap formation. Using eq. (8) and the above approximations, the continuity equation (eq. 5) becomes

$$\dot\gamma\delta\frac{\partial\delta}{\partial x}=-\Gamma, \qquad (11)$$

and the momentum balance equation (eq. 6) together with eq. (7) simplifies to

$$\dot\gamma^2\delta\frac{\partial\delta}{\partial x}=-\frac{g\sin(\beta_m-\beta)}{\cos\beta_m}. \qquad (12)$$

Combining eqs. (11) and (12) yields

$$\Gamma=\frac{g\sin(\beta_m-\beta)}{\dot\gamma\cos\beta_m}, \qquad (13)$$

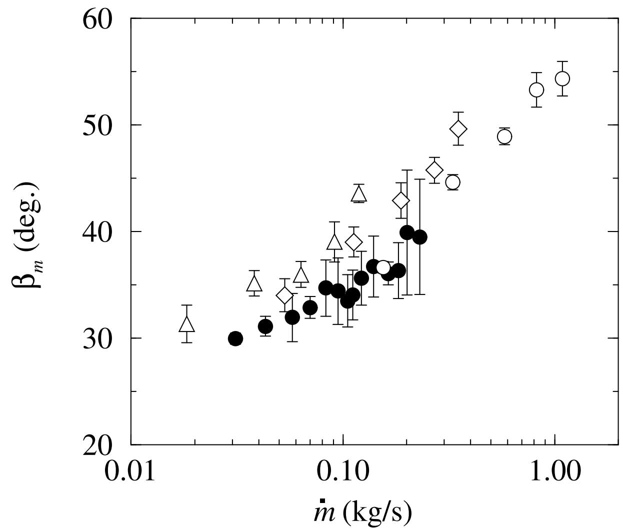

FIG. 2: Variation of the maximum angle of repose (β_m) with mass flow rate ($\dot{m}$) for 2 mm steel balls. Filled symbols: open heap system [19]. Open symbols: rotating cylinder system for three cylinder sizes [30].

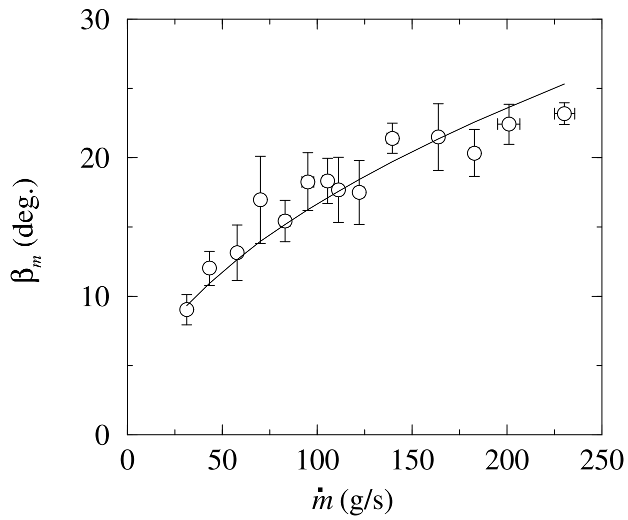

FIG. 3: Variation of the layer thickness (δ) with mass flow rate ($\dot{m}$) for 2 mm steel balls in an open heap system. The solid line is a best fit of the form $\delta \propto \dot{m}^{1/2}$.

which, for the case when $\beta_m \approx \beta$, reduces to

$$\Gamma \approx V(\beta_m - \beta), \tag{14}$$

where $V = g/\dot{\gamma}\cos\beta_m$. Thus, the continuum model yields a source term similar to the BRdG model; the scaling of V is also similar to the BRdG model.

We further simplify the above equations for two different geometries of heap formation: *closed*, as shown in Fig. 1a, and *open* in which the end wall (E, Fig. 1a) is removed. Consider the open system first. In this case, at steady state, all the material entering the system leaves at the far edge of the heap and no particles are absorbed or eroded. This implies that $\Gamma = 0$, which on substituting into eq. (13) yields $\beta = \beta_m \equiv$ constant. Using these results in eqs. (11) and (12) shows that the average velocity (u) and thickness (δ) of the flowing layer are also constant in open systems. The mass flow rate in the system is given by $\dot{m} = \rho u \delta T$, where T is the width of the layer. This expression, together with eq. (8), gives the following relationship between the layer thickness and mass flow rate

$$\delta = \left[2\dot{m}/(T\rho\dot{\gamma})\right]^{1/2}. \tag{15}$$

Thus, the model indicates that in open systems a non-accelerating flowing surface layer with a uniform thickness is obtained, and the interface angle is equal to the maximum angle of repose.

Experimental results of Khakhar *et al.* [19] based on flow visualization studies validate the above predictions, and sample results are given below. Fig. 2 shows the variation of the maximum angle of repose with mass flow rate in the system for 2 mm steel balls in an open heap system (filled symbols). The data indicate that β_m, and thus the coefficient of static friction at the heap-layer interface ($\tan\beta_m$), is not a constant but increases with the local flow rate. An increase in surface angle with flow rate was also reported by Lemieux and Durian [29]. Zhang and Cambell [31] found the Mohr-Coulomb criterion with a constant coefficient of friction to be valid in their 2d simulations of sheared spheres in a gravity field. In contrast, Daerr and Douady [27] reported an exponential decrease in the coefficient of static friction with layer thickness for particles initially at rest on a plane surface. Fig. 3 shows the variation of the layer thickness (δ) with mass flow rate. The solid line is a fitted curve of the form $\delta \propto \dot{m}^{1/2}$. This indicates agreement with theoretical predictions (eq. 15) if the product $\rho\dot{\gamma}$ is independent of mass flow rate.

Consider next the application of the quasi-steady-state model results to heap formation in a closed system (Fig. 1a). At steady state we must have $\Gamma \equiv$ constant for the heap to rise uniformly. Integrating eq. (11), the layer thickness profile is obtained as

$$\delta = \left[\delta_L^2 + 2\Gamma(L-x)/\dot{\gamma}\right]^{1/2} \tag{16}$$

where δ_L is the layer thickness at the end of the layer, $x = L$, and L is the length of the interface (Fig. 1a). The rise velocity is related to the mass flow rate by

$$\Gamma = \dot{m}/(TL\rho), \tag{17}$$

and the interface angle calculated from eq. (14) is

$$\beta = \beta_m - \Gamma/V. \tag{18}$$

Experimental results of Khakhar *et al.* [19] for closed systems show that the rise velocity (Γ) varies nearly linearly with mass flow rate in agreement with eq. (17),

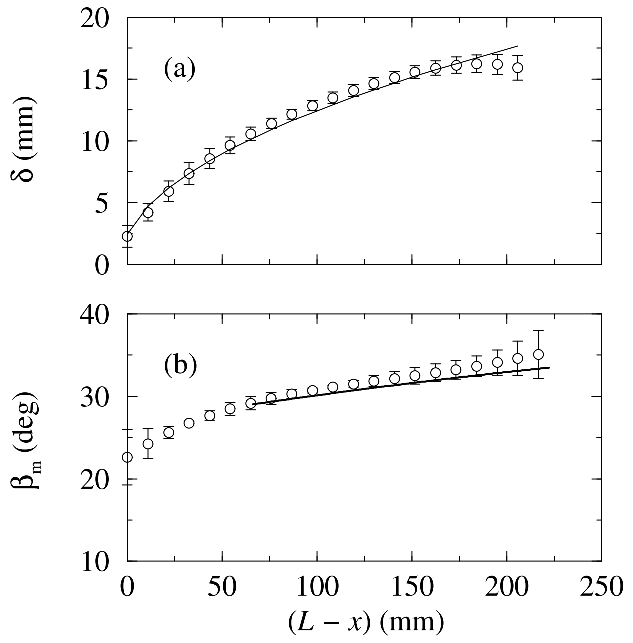

FIG. 4: Variation of the (a) layer thickness (δ) and (b) surface angle (β) with distance from the edge of the heap ($L-x$) for flow of 2 mm steel balls in a closed system. Symbols are experimental data and error bars indicate the standard deviation over six measurements. Solid line in (a) is a fit of eq. (16) and in (b) is the prediction of eq. (17).

and the density, which is found to be constant, is $\rho = 3.2$ g/cm^3. Fig. 4 shows the variation of both layer thickness (δ) and interface angle (β) with length along the bed-layer interface ($L-x$) for a fixed mass flow rate. The solid line in Fig. 4a is a fit of eq. (16) to obtain δ_L and $\dot{\gamma}$. There is a good match between the fitted line and the experimental data, which suggests that the shear rate, $\dot{\gamma}$, is constant. Similar results are obtained for all flow rates studied. Using experimental results for the rise velocity (Γ) and the interface length (L), we obtain $\dot{\gamma} = 20 \pm 2$ s^{-1} from eq. (16), where the standard deviation indicated is calculated for all 10 flow rates studied. Using the value of the bulk density obtained above, we find from eq. (15) that the shear rate for the open system is $\dot{\gamma} = 22 \pm 3$ s^{-1}. The value of the shear rate predicted from eq. (9) is $\dot{\gamma} = 20 \pm 5$ s^{-1} for the range of mass flow rates considered. Thus the shear rates for the open and closed systems are the same within experimental error, and predictions of theory are in reasonable agreement with experimental values.

IV. ROTATING CYLINDER

The simplest case corresponds to rotating cylinder flow, for 50% fill fraction. Assuming a nearly flat interface, the source term is given by $\Gamma = \omega x$. Subsituting into the continuity equation (eq. 5) and integrating we obtain

$$u\delta = \frac{\omega}{2}\left(L^2 - x^2\right). \tag{19}$$

Using eq. (5) the momentum balance equation (eq. 6) simplifies to

$$u\frac{du}{dx} = \frac{3g}{4}\frac{\sin(\beta-\beta_s)}{\cos\beta_s} - 3\frac{cdu^2}{\delta^2} + \frac{\omega x u}{\delta}. \tag{20}$$

We consider two different limiting solutions to eqs. (19) and (20) below.

Firstly, consider the case when shear rate ($\dot{\gamma}$) is nearly constant. Using eq. (8), the flux equation (eq. 19) gives the layer thickness profile as

$$\delta = \left(\frac{\omega}{\dot{\gamma}}\right)^{1/2}\left(L^2 - x^2\right)^{1/2}, \tag{21}$$

which is symmetric for all rotational speeds (ω). Eq. (21) corresponds to the model of Makse [17], in which the shear rate is assumed to be a fitting parameter. In the present case the shear rate is obtained from eq. (9). The mean velocity in this case is given by

$$u = \left(\frac{\omega\dot{\gamma}}{4}\right)^{1/2}\left(L^2 - x^2\right)^{1/2}. \tag{22}$$

Substituting these results in eq. (20), and using the Mohr-Coulomb condition (eq. 7) yields eq. (13) with $\Gamma = \omega x$. This allows for calculation of the angle (β) along the interface. Thus the assumption of a constant shear rate is consistent with the model, and gives a complete description of the flow in terms of $\bar{u}(\xi)$, $\bar{\delta}(\xi)$ and $\beta(\xi)$, where ξ is the dimensionless distance along the interface in the flow direction. However, it is not apparent from the analysis, under what conditions the solution is valid.

Consider next the case when the shear rate is not constant along the layer. We obtain a solution here for the case when acceleration (du/dx) is small. Scaling is used to determine conditions when this approximation is valid. Eliminating δ using eq. (19), the scaled momentum balance becomes

$$\bar{u}\frac{d\bar{u}}{d\xi} = \frac{3}{4Fr}\frac{\sin(\beta-\beta_s)}{\cos\beta_s} - 12cs\frac{\bar{u}^4}{(1-\xi^2)^2} + \frac{2\xi\bar{u}^2}{1-\xi^2}, \tag{23}$$

where $\bar{u} = u/\omega L$, $\xi = x/L$ and the dimensionless parameters are the Froude number, $Fr = \omega^2 L/g$, and the size ratio, $s = d/L$. The first term on the right hand side of eq. (23) is the net driving force, that is the gravitational force less the frictional resistance to flow. This term is independent of the flow velocity ($\bar{u}$). The second term is the 'viscous' resistance due to collisional stresses, and the third term arises as a result of in-flow and out-flow of particles from the layer. Both these terms depend on the flow velocity. Typical experimental Froude numbers for experiments in rotating cylinders are in the range $O(10^{-3})$ to $O(10^{-2})$. In these cases the driving force term $(O(1/Fr))$ is much larger than the acceleration term $(O(\xi/\sqrt{sFr})$ based on eq. 22), particularly near the midpoint of the layer ($\xi = 0$). The collisional stress term is of the same magnitude as the net driving force term since the flow velocity increases to balance the two. Thus for $\xi\sqrt{Fr/s} \ll 1$ the acceleration term may be neglected.

For negligible acceleration ($d\bar{u}/d\xi \approx 0$), the scaled mean flow velocity is obtained from eq. (23) as

$$\bar{u} = \left(\frac{1-\xi^2}{12cs}\right)^{1/2} \left[\xi + (\xi^2 + 9csA/Fr)^{1/2}\right]^{1/2}, \quad (24)$$

where $A = \sin(\beta - \beta_s)/\cos\beta_s$. Using eq. (19), scaled the layer thickness profile is

$$\bar{\delta} = \left[\frac{3cs(1-\xi^2)}{\xi + (\xi^2 + 9csA/Fr)^{1/2}}\right]^{1/2}, \quad (25)$$

where $\bar{\delta} = \delta/L$. The above solution is valid only if $A > 0$, that is if $\beta > \beta_s$. For $\beta \le \beta_s$, we have $\bar{u} = \bar{\delta} = 0$, thus there is no steady flow possible if the interface angle is less the static angle of repose. This is consistent with the definition of the static angle of repose. Note that the layer profile is not symmetric about $\xi = 0$, and for any $\xi > 0$ we have $\bar{\delta}(-\xi) > \bar{\delta}(\xi)$, that is, the upper part of the layer ($\xi < 0$) is thicker than the lower part. The source of the asymmetry is the in-flow/out-flow term in the momentum balance (third term on the right hand side of eq. 23). In the upper part of the layer ($\xi < 0$) the flow is retarded by material entering the layer from the bed ($\Gamma < 0$) and the reverse is true in the lower part of the layer. Thus, the layer is thicker in upper part because of the lower velocity relative to the lower part of the layer ($\xi > 0$), resulting in a skewed profile. Further, eq. (25) indicates that the profile becomes more skewed with increasing Froude number (Fr) and decreasing size ratio (s). In the limit, $Fr/s \ll 1$, the scaled layer thickness profile becomes

$$\bar{\delta} = \left(\frac{csFr}{A}\right)^{1/4} (1-\xi^2)^{1/2}, \quad (26)$$

which is identical to the result obtained assuming a constant shear (eq. 21) when eq. (9) is used to calculate the shear rate. This implies that a profile symmetric about the layer midpoint ($\xi = 0$) is obtained at very low Froude numbers and relatively high size ratios, and in this limit the shear rate is nearly constant as shown below.

The shear rate obtained using eq. (8) and the expressions for mean velocity and layer thickness for negligible acceleration (eqs. 24,25) is

$$\dot{\gamma}(\xi) = \frac{\omega}{3cs}\left[\xi + (\xi^2 + 9csA/Fr)^{1/2}\right]. \quad (27)$$

In the limit, $Fr/s \ll 1$, we obtain $\dot{\gamma} = \omega(A/csFr)^{1/2}$, which is eq. (9) in scaled form.

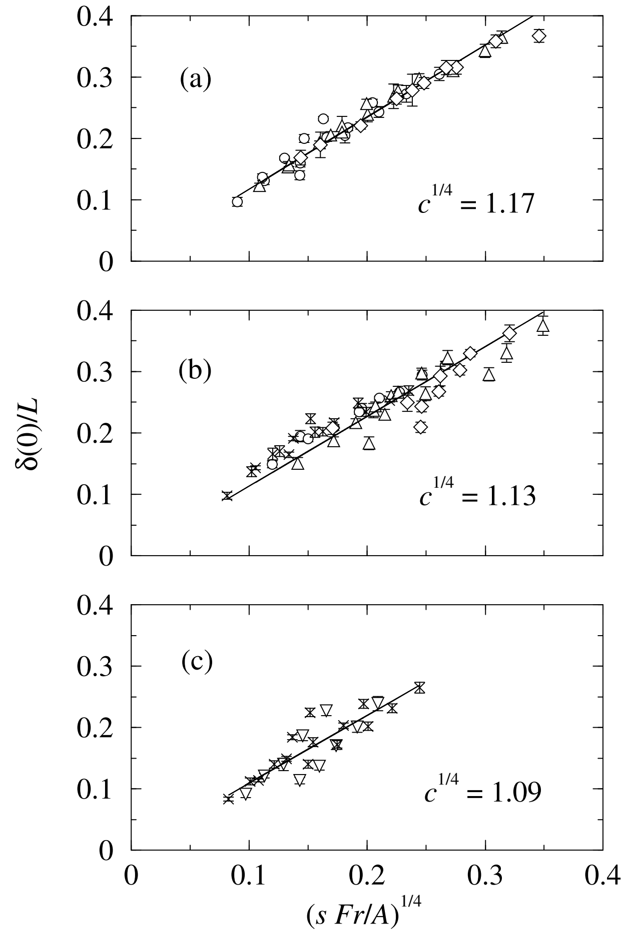

FIG. 5: Variation of the layer thickness at the midpoint ($\delta(0)$) with $(sFr/A)^{1/4}$ for (a) steel balls, (b) glass beads (c) and sand particles in cylinders of different sizes and at different rotational speeds. Symbols are experimental data for different sized particles: $\circ$ $d = 1$ mm, $\triangle$ $d = 2$ mm, $\diamond$ $d = 4$ mm, $\triangledown$ $d = 0.4$ mm and $\times$ $d = 0.8$ mm. The solid line is a fit of eq. (27) and the values of the parameter $c^{1/4}$ are indicated.

Calculation of the layer thickness profile requires an estimate for the parameter A which depends on the interface angle profile ($\beta(\xi)$). From eq. (14), using $\Gamma = \omega x$ and eq. (9), we obtain interface angle profile in terms of the scaled variables as

$$\beta(\xi) = \beta_m - \frac{Fr\cos\beta_m}{3cs}\left[\xi + (\xi^2 + 9csA/Fr)^{1/2}\right]\xi. \quad (28)$$

In simplifying the preceding equation we assume $\beta_m \approx \beta \approx \beta_s$, as above. Eq. (28) indicates that the interface angle decreases monotonically with distance along the interface and at $\xi = 0$, $\beta = \beta_m$. Thus in the rotating cylinder flow the maximum angle of repose can be experimentally obtained by measuring the interface angle at the midpoint of the layer. For $(Fr/s)\xi$ sufficiently large and $\xi > 0$, we get $\beta < 0$, that is, for small size ra-

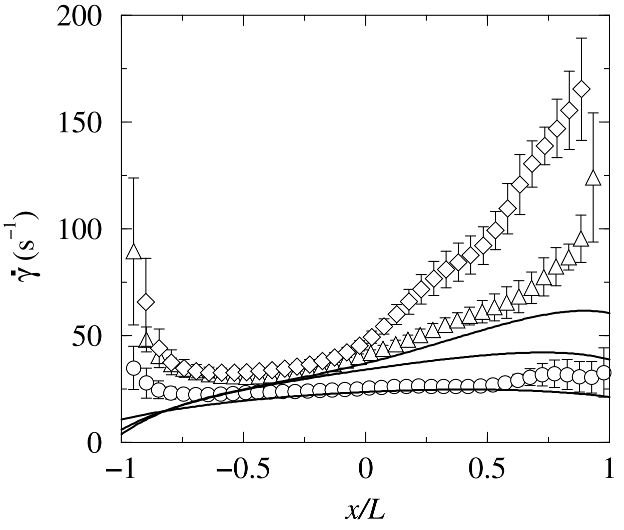

FIG. 6: Variation of the shear rate ($\dot{\gamma}$) along the flow direction for 2 mm steel balls in cylinder of radius $R =$ 16 cm. Symbols show data for three different Froude numbers (Fr): $\circ$ $Fr = 2 \times 10^{-3}$, $\triangle$ $Fr = 22 \times 10^{-3}$, $\diamond$ $Fr = 64 \times 10^{-3}$. Solid lines are the predictions of the eq. (27).

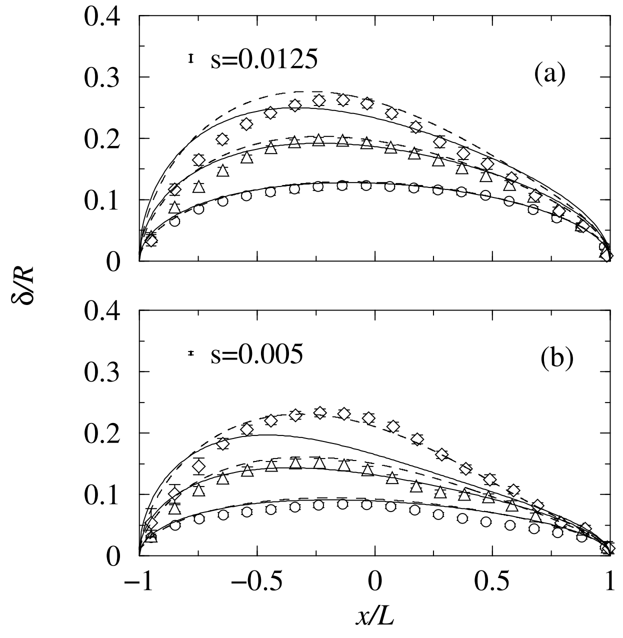

FIG. 7: Layer thickness profiles for (a) 2 mm steel balls and (b) 0.8 mm sand. Symbols denote experimental data for three different froude numbers (Fr): $\circ$ $Fr = 2 \times 10^{-3}$, $\triangle$ $Fr = 22 \times 10^{-3}$, $\diamond$ $Fr = 64 \times 10^{-3}$. Solid lines are predictions of eq. (25) and dashed lines are the predictions of the model of Khakhar *et al.* [13]. The error bars give the standard deviation over 6 measurements and the bar indicates the scaled diameter of a particle ($s = d/R$).

tios and large Froude numbers the layer profile may turn up at the end. Conversely, when $(Fr/s) \ll 1$, eq. (28) yields $\beta \approx \beta_m$, and the interface profile is nearly flat. Neglecting terms $O(\xi Fr/s)$, which is consistent with the approximation in the momentum balance equation, the parameter A is

$$A = \frac{\beta_m - \beta_s}{\cos \beta_s}. \tag{29}$$

The above result implies that we may take A to be nearly constant and based on the interface angle at the midpoint of the layer. This approximation was used in the analysis given by Khakhar *et al.* [13], but without the above justification.

Consider next a comparison of the theoretical results to experimental data. A few key numbers are reported, as they convey a sense of qualitative agreement. However, for full details the reader is referred to [30] and [19]. The model parameters required are β_s, β_m and c, as in the case of the heap. Data of Orpe and Khakhar [30] for the first two parameters are shown in Fig. 2 for 2 mm steel balls in rotating cylinders of 3 sizes and for different rotational speeds of the cylinders. The data correlates reasonably well with the mass flow rate at the midpoint of the layer calculated from $\dot{m} = \rho \omega L^2 T/2$, where T is the cylinder length and the same density as in the heap experiments ($\rho = 3.2$ g/cm^3) is used. Data spanning nearly two decades of flow rate fall on a single curve, although with some scatter. The maximum angle of repose increases with mass flow rate, and the measured values are similar to those from heap experiments which are also shown in the same figure. The static angle of repose is the angle at $\dot{m} = 0$.

Orpe and Khakhar [30] had obtained $c \approx 1.5$ by fitting the theory of Khakhar *et al.* [13] to experimental layer thickness profiles. We obtain a new estimate of the parameter based on the layer thickness at the midpoint of the layer ($\xi = 0$), which, from eq. (25), is $\bar{\delta}(0) = (csFr/A)^{1/4}$. Fig. 5 shows experimental data for $\bar{\delta}(0)$ versus $(sFr/A)^{1/4}$ for experimental data for 90 experiments comprising steel balls, glass beads and sand of different sizes in cylinders of different sizes and for different rotational speeds. The data falls on a straight line for each material (although with some scatter) and a least squares fit gives $c = 1.9$ for steel balls, $c = 1.6$ for glass beads and $c = 1.4$ for sand. Since the model is essentially exact at $\xi = 0$, the good fit implies that the proposed constitutive equation for stress is reasonable, and the shear rate in the layer is well-described by eq. (27) at $\xi = 0$. However, the variation of the shear rate with distance (ξ) is underpredicted by the theory (eq. 27) as shown in Fig. 6.

Predictions of the model for the layer thickness profile are compared to experimental data in Fig. 7 for sand particles and steel balls for different Froude numbers in

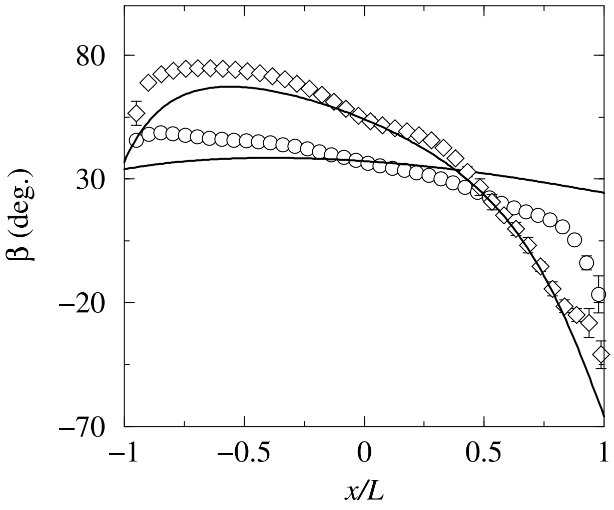

FIG. 8: Variation of the interface angle (β) along the flow direction for 2 mm steel balls in cylinder of radius $R = 16$ cm. Symbols show data for two different Froude numbers (Fr): $\circ$ $Fr = 2 \times 10^{-3}$ and $\diamond$ $Fr = 64 \times 10^{-3}$. Solid lines are the predictions of the eq. (28).

a cylinder of radius 16 cm, using the value of c obtained above and experimental values for β_m and β_s. The agreement is good except at the highest Fr and low s, and the all the qualitative features of the data are reproduced. At low Fr and relatively high s studied, the profile is nearly symmetric (steel balls at the lowest Fr), and the profiles become more skewed with increasing Fr and decreasing s. The deviation at the high Froude numbers and low size ratio are due to neglect of the acceleration term. Similar agreement is obtained for the other cases studied as well. The predictions of the model of Khakhar *et al.* [13] are shown in the figure as dashed lines. These nearly coincide with the results from the present model, except for the highest Fr for sand, indicating that the approximations made are reasonable for the parameter values of interest. It is remarkable that such a simple theory is able to describe the behavior of the system over such a wide range of parameters: materials include steel balls, glass beads and sand; varying shapes with steel balls being spherical, glass beads, nearly spherical and sand being irregularly shaped; size ratios in the range $s \in (0.005, 0.05)$ and Froude numbers in the range $Fr \in (2 \times 10^{-3}, 64 \times 10^{-3})$.

Consider finally the predictions of the model for shape of the interface. Fig. 8 shows a comparison between the measured interface angles (β_x) and the angles predicted from eq. (28). The experimentally measured values of β_m are used in the calculation. There is reasonable agreement between the theory and experiment except at the highest Fr, but significant deviations are obtained at lower Fr. Notice that the surface angle becomes negative for both experiments and theory at high Fr. This corresponds to a turning up of the interface at the end of the layer producing the characteristic S-shape (see layer

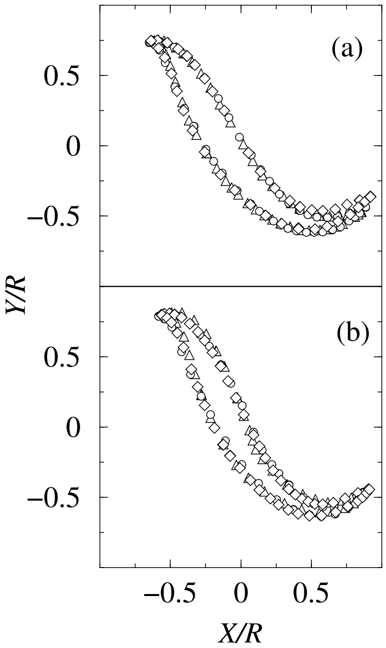

FIG. 9: Layer shape profiles for different materials in cylinders of different sizes for $Fr = 64 \times 10^{-3}$. (a) Steel balls and glass beads with $s = 0.0125$, $\circ$ steel balls with $R = 16$ cm, $\triangle$ steel balls with $R = 8$ cm, $\diamond$ glass beads with $R = 16$ cm. (b) Sand and glass beads with $s = 0.00475$, $\circ$ sand with $R = 16$ cm, $\triangle$ sand with $R = 8$ cm, $\diamond$ glass beads with $R = 16$ cm.

shape profiles in Fig. 9). Similar behaviour is obtained for glass beads and sand.

An implication of the scaling shown in Fig. 5 is that the flow in the layer primarily depends on the Froude number and size ratio and material poperties have a secondary effect. This indeed is observed in experiments. Fig. 9 shows superimposed layer shape profiles for cylinders of different sizes and different materials such that Fr and s are constant in each case. The profiles are nearly identical indicating good scaling. Such scaling is explored in more detail in ref. [30].

V. CONCLUSIONS

A theoretical framework serves to unify the behaviour of surface flows for two prototypical systems: heap flow and rotating cylinder flow. The model is based on a stress constitutive equation and failure criterion which contain three material parameters: β_s, β_m and c. Analytical results for both systems give a complete description of the systems in terms of the layer thickness profiles ($\delta(x)$), average velocity of flow ($u(x)$) and the interface angle profile ($\beta(x)$). In open heap systems a layer of uniform thickness with a uniform flow velocity is obtained, whereas in the closed heap system $\delta^2 \propto x$. The interface angle is constant and equal to the maximum angle of repose in the open system, whereas it decreases with distance from the pouring point in the closed system. Results for the rotating cylinder are obtained for the case when the acceleration of particles in the layer is small ($\xi\sqrt{Fr/s} \ll 1$). The layer profile is found to be asymmetric about the midpoint of the layer ($\xi = 0$) with the upper part of the layer ($\xi < 0$) being thicker. The skewness increases with increasing Froude numbers and decreasing size ratios. The scaled shear rate ($\dot{\gamma}/\omega$) decreases with increasing Froude number and size ratio, and for a given case it increases with distance along the layer. The layer interface angle decreases with distance in the flow direction. For high $\xi Fr/s$ and $\xi > 0$ the layer turns up, whereas when $\xi Fr/s$ is small a nearly flat interface is obtained.

Quasi-2d experiments carried out for open and closed heaps and rotating cylinders of different sizes, by and large, validate the predictions of the theory. Deviations from experimental data appear in the shear rate profile and the interface angle profile in the rotating cylinder flow. Both these factors are most likely due to end wall effects which are discussed below.

The theory presented here is based on two stress constitutive equations: one for the shear stress in the flow layer and the second for the shear stress at the bed layer interface. The model has three material parameters (β_s, β_m and c), and all three parameters can be obtained from relatively simple experimental measurements. Experiments support the validity of equations (granular layer flowing on the surface of a static heap), and these equations can be applied to more complex geometries.

The experimental results presented here are all based on quasi-2d systems with gaps ranging from 5-25 particle diameters. Thus, wall effects are important and unavoidable in the experimental technique used (flow visualization). Rotating cylinder experiments [30] indicate that the walls have an insignificant effect on the flow (that is the mean velocity and layer thickness profiles) but significantly affect the interface angles. Thus, the accuracy of the measured values of the parameters β_s and β_m is in question. It is not surprising that the theory does not give good predictions of the shear rate and interface angle profiles because both these depend strongly on $\beta_m(\dot{m})$. Clearly, for a more accurate determination of material parameters experiments on 3d systems are necessary.

ACKNOWLEDGMENTS

D. V. Khakhar acknowledges the financial support of the Department of Science and Technology, India, through the Swarnajayanti Fellowship project (DST/SF/8/98) for part of this work. This work was supported in part by grants to J. M. Ottino from the Division of Basic Energy Sciences of the Department of Energy, the National Science Foundation, Division of Fluid and Particulate Systems, and the Donors of the Petroleum Research Fund, administered by the American Chemical Society.

REFERENCES

[1] C. S. Campbell, Annu. Rev. Fluid Mech. **22**, 57, (1990).
[2] H. M. Jaeger, S. R. Nagel, and R. P. Behringer, Rev. Mod. Phys. **68**, 1259, (1996).
[3] J. Duran, Powder and Grains, Springer-Verlag, NewYork, (2000).
[4] G. H. Ristow, Pattern Formation in Granular Materials, Springer, Berlin, (2000).
[5] J. M. Ottino and D. V. Khakhar, Annu. Rev. Fluid Mech. **32**, 55, (2000).
[6] B. J. Ennis, J. Green, and R. Davis, Chem. Eng. Prog. **90**, 32, (1994)
[7] J. Bridgewater, Chem. Eng. Sci. **50**, 4081, (1995).
[8] P. G. de Gennes, Rev. Mod. Phys. **71**, S374, (1999).
[9] J. Rajchenbach, Phys. Rev. Lett. **65**, 2221, (1990).
[10] S. J. Rao, S. K. Bhatia, and D. V. Khakhar, Powder Technol. **67**, 153, (1991).
[11] O. Zik, D. Levine, S. G. Lipson, S. Shtrikman, and J. Stavans, Phys. Rev. Lett. **73**, 644, (1994).
[12] J. P. Bouchaud, M. Cates, J. Ravi Prakash and S. Edwards, J. Phys. France I, **4**, 1383, (1994).
[13] D. V. Khakhar, J. J. McCarthy, T. Shinbrot, and J. M. Ottino, Phys. Fluids, **9**, 31, (1997).
[14] A. A. Boateng and P. V. Barr, J. Fluid Mech. **330**, 233, (1997).
[15] T. Elperin and A. Vikhansky, Europhys. Lett. **42**, 619, (1998).
[16] T. Boutreux, E. Raphaël, and P. G. de Gennes, Phys. Rev. E, **58**, 4692, (1998).
[17] H. A. Makse, Phys. Rev. Lett. **83**, 3186, (1999).
[18] S. Douady, B. Andreotti and A. Daerr, Eur. Phys. J. **11**, 131, (1999)
[19] D. V. Khakhar, A. V. Orpe, P. Andresén and J. M. Ottino, J. Fluid Mech. **441**, 255, (2001).
[20] R. A. Bagnold, Proc. R. Soc. London Ser. A, **255**, 49 , (1954).
[21] H. Henein, J. K. Brimacombe, and A. P. Watkinson, Metall. Trans. B, **14B**, 191, (1983).
[22] M. Nakagawa, S. A. Altobelli, A. Caprihan, E. Fukushima, and E. K. Jeong, Exp. Fluids, **16**, 54, (1993).
[23] J. Rajchenbach, E. Clément, and J. Duran, in *Fractal Aspects of Materials*, edited by F. Family, MRS Symposium Proceedings No. 367 (Materials Research Society, Pittsburgh, 1995), p. 525.
[24] C. M. Dury, G. H. Ristow, J. L. Moss, and M. Nakagawa, Phys. Rev. E, **57**, 4491, (1998).
[25] K. Yamane, M. Nakagawa, S. A. Altobelli, T. Tanaka, and Y. Tsuji, Phys. Fluids, **10**, 1419, (1998).

[26] J. Rajchenbach, in *Physics of Dry Granular Media*, edited by H. Hermann (Kluwer Academic, Dordrecht, 1998), p. 421.
[27] A. Daerr, S. Douady, Nature, **399**, 241 (1999).
[28] R. Khosropour, E. Valachovic, and B. Lincoln, Phys. Rev. E, **62**, 807, (2000).
[29] P. -A. Lemieux, D. J. Durian, Phys. Rev. Lett. **85**, 4273 (2000).
[30] A. V. Orpe and D. V. Khakhar, D. V., Scaling relations for granular flow in quasi-2d rotating cylinders, submitted to Phys. Rev. E (in press).
[31] Y. Zhang, C. S. Campbell, J. Fluid Mech., **237**, 541 (1992).